# Stabilizing water films using surface acoustic waves

Amihai Horesh, Anna Zigelman, and Ofer Manor[*]

*Wolfson Department of Chemical Engineering, Technion-Israel Institute of Technology, Haifa 32000, Israel*

Stabilizing and destabilizing films of liquid by design is not a simple challenge to overcome. Megahertz-frequency surface acoustic waves (SAWs), which propagate in a solid substrate, may stabilize liquid films against capillary forces, which otherwise promote the film breakup and the dewetting of the substrate. Here we explore the contribution of SAWs to the dynamics of micron- and submicron-thick films of water, which intervene between a bubble and a solid substrate. The investigation in this paper was inspired by a previous theoretical work on the acoustic Landau-Levich coating problem, which predicts the onset of stable and unstable coating films under the excitation of SAWs. We observe that the parametric regime of the stable Landau-Levich coating film translates to stable water films in our experiments. Moreover, we observe that unlike previous experiments with silicon oil, water films do not collapse under the parametric regime of the unstable Landau-Levich coating film, but appear to remain stable. A key to this controversy appears to be the presence of the stabilizing, long range, electrical double layer force in water, which is anticipated to alter the film response to the SAW.

## I. INTRODUCTION

Stable and unstable films of liquid usually appear in the context of stabilizing and destabilizing colloidal suspensions [1–3] and in the context of avoiding bubble or drop pinning to the walls of microfluidic channels [4] in colloid science and in microfluidics, respectively. The attachment and pinning of a bubble to the wall of a solid substrate occurs following the drainage of liquid from the intervening liquid film between the bubble and the channel wall [5,6]. The intervening liquid film thins until rupture [7].

When it comes to microfluidics, attempts to stabilize liquid films mostly originate from the necessity to avoid channel clogging by bubbles and other soft matter particles that pin to the channel walls. Kohnle *et al.* [4] and Litterst *et al.* [8] studied how the geometry of a T-junction configuration may prevent bubbles from clogging on microchannel walls. Hibara *et al.* [9] developed the capillarity restricted modification (CARM) method to generate controlled patterns of hydrophilic and hydrophobic microchannels with different thicknesses which are aimed at preventing bubble pinning. Moreover, the use of hydrophobic/hydrophilic microfluidic systems was widely studied to improve the efficiency of bubble removal in microfluidic systems. Xu *et al.* [10] presented both experimentally and theoretically how the use of a membrane surface can separate between a bubble and the liquid on microfluidic platforms. Derami *et al.* [11] designed different sized pore platforms from four different polytetrafluoroethylene membranes to remove bubbles from a water-filled microchannel in a T-junction configuration. Another interesting technique was studied by Zheng *et al.* [12] and Lochovsky *et al.* [13], who removed bubbles by using in-line bubble

---

[*]manoro@technion.ac.il

trapping. They reported that this technique was found to be highly effective for long term bubble removal. Moreover, Chen *et al.* [14] used a carrier immiscible liquid as a spacer to separate between liquid droplets and the walls of a microchannel. Besides mechanical aspects, also chemical approaches were tested aiming at avoiding pinning of bubbles or droplets to surfaces. The most common method to change the surface chemistry of elastomeric and glass microchannels is the use of plasma and in particular air or oxygen plasma to render the channel wall hydrophilic, stabilizing the presence of the carrier liquid, which is usually water [15]. Another approach is to coat the channel wall with a hydrophobic or hydrophilic layer, which was used to maintain the stability of emulsions [16]. The common denominator of the different mechanical and chemical methods given above is that they are all passive.

Recently, Morozov and Manor [17] studied the Landau-Levich coating problem, where megahertz-frequency surface acoustic waves (SAWs) support the dynamic coating of a solid surface by a liquid film, which is extracted from a reservoir. It was found that the stability of the film is determined by a balance between the acoustic and capillary stresses in the liquid. The balance is quantified by the acoustic Weber number, $We_s$. Large acoustic stresses ($We_s > 1.49$) were found to support stable continuous coating films. Large capillary stresses ($We_s < 1.49$) were found to yield the collapse of the coating film which results in the dewetting of the solid substrate. The same nondimensional parameter was used previously to analyze the dynamic wetting of water/surfactant mixtures under the excitation of SAWs [18,19], and was employed later to study the stability of air bubbles in silicon oil in microfluidic channels [20]. In the latter study, the dynamics of a silicon oil film, which intervened between a bubble and a solid substrate, was found to be similar to the dynamics of the coating film in the Landau-Levich coating problem for the explored cases that satisfied large capillary stresses ($We_s < 1.49$). In particular, the collapse rate of the oil film was enhanced by several orders of magnitude under the action of the SAW relatively to the corresponding case in the absence of the SAW. Moreover, a recent analysis of the equations, which govern the acoustic Landau-Levich coating problem, further shows a plethora of nonlinear coating phenomena at smaller levels of $We_s$ and film thicknesses [21].

Here we discuss the contribution of a megahertz-frequency SAW, which propagates in a solid substrate of a 500-micron-thick channel, to the stabilization of a micron and submicron intervening film of water between the substrate of the channel and a long bubble therein. In what follows, we explain the experimental setup in Sec. II, show and discuss our findings in Sec. III, and conclude in Sec. IV.

## II. EXPERIMENTAL SYSTEM

We designed an acoustomicrofluidic system that consists of an acoustic actuator (SAW device) and a microfluidic channel. The acoustic actuator is made of a 0.5 mm 128° y-cut lithium niobate (LN) piezoelectric crystal. We used photolithography techniques to fabricate 1-$\mu$m aluminum atop a 10-nm titanium interdigitated transducer (IDT), respectively, on the LN substrate [22]. To support a MHz SAW, each electrode in the IDT was set to be 50 $\mu$m wide and 50 $\mu$m apart from the next electrode. The 500-$\mu$m-thick channel, which we fabricated on the acoustic actuator, includes a T junction to merge streams of water and air in order to obtain long bubbles in the channel [23]. The microchannel master mold was designed and prepared using a computer numerical control (CNC) technique. The mold was covered by polydimethylsiloxane (PDMS), in a weight ratio of 1:10, and cured for 24 hours, where during the last 2 hours it was kept at a temperature of 100°C. The microchannel system within the PDMS was attached to the LN surface using oxygen plasma [24], and was immediately filled with deionized (DI) water. In Fig. 1(a) we show a schematic illustration of our acoustomicrofluidic system. We connected the IDT to a signal generator [25] and an amplifier [26] to generate SAWs. By scanning the SAWs on the LN substrate using a laser Doppler vibrometer [27], we verified that the SAW is a propagating wave and that the amplitude of the transverse particle velocity of the SAW at the LN surface was in the range $U = 94.5$–$313$ mm/s
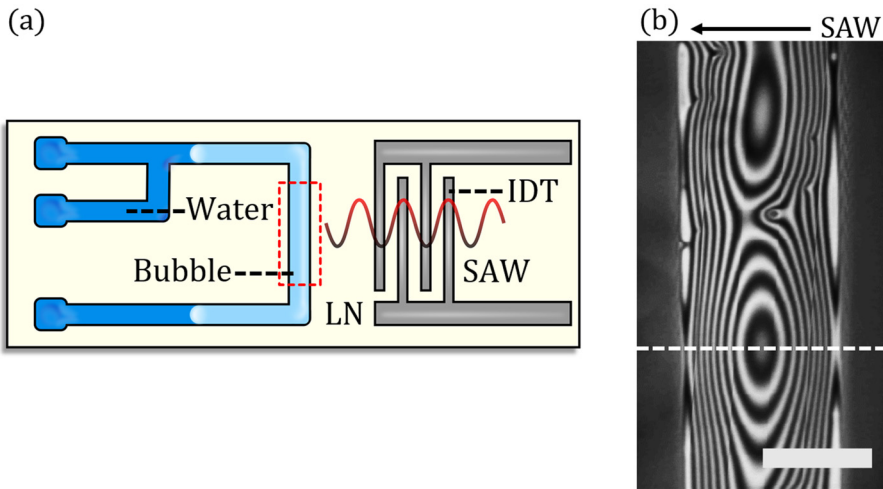
FIG. 1. (a) A schematic illustration of the experimental setup, showing a microfluidic channel on the left and an interdigitated transducer (IDT), which generates propagating SAWs in the lithium niobate (LN) substrate, on the right. We use light microscopy to image the area enclosed by the dashed red square which gives (b) a top view of the light fringes, generated in the intervening water film between the bubble and the LN substrate; the scale bar is 100 $\mu$m.

in our experiments, noting that the corresponding exact SAW frequency was 19.893 MHz. The measured range of amplitude velocities is common for SAW microfluidic applications [28].

We pumped DI water into the microchannel at a flow rate of 3 $\mu$l/min and air at a flow rate of 27 $\mu$l/min, using syringe pumps [29]. These flow rates allowed us to produce long bubbles in the channel. When the rate of bubble generation reached a steady state, we stopped the system and stabilized the pressure inside the channel by exposing the inlet and outlet ports to atmospheric pressure. We used an inverted microscope [30], and a 10× magnification lens (overall microscope magnification of 100×) with a focus depth of ∼10 $\mu$m [31], in addition to a monochromatic camera [32] and a monochromatic light source (light wavelength transmission of 436 ± 10 nm) to capture the dynamics of the liquid film (sandwiched between the bubble and the LN substrate) in the absence and in the presence of SAW excitation. Moreover, since the focus depth employed was smaller than the thickness of the channel, it was not sufficiently large to cover the whole channel height. In order to focus the microscopic lens on the intervening film near the bottom of the channel, we first focused the lens at the bottom wall of the channel and then slowly raised the focus upward until light fringes, which originate from the diffraction of light in the liquid film, came into view.

The constructive and destructive interference of the monochromatic light in the film appears in the microscope images as bright and dark fringes, respectively, as is shown in Fig. 1(b). Based on the analysis of Wong *et al.* [33], it is known that without the application of a SAW, the thickness profile of the intervening liquid film between the bubble and the solid substrate is a convex parabola, at least while the bubble is moving in the channel and shortly after the motion of the bubble is arrested. The film geometry is sketched in the red dashed square in Fig. 2(a) and magnified in Fig. 2(b). Further, according to our experimental observation, the qualitative geometry of the film remains approximately the same throughout the experiment, albeit the thickness of the film appears to change. We reconstructed the spatiotemporal variations of the film thickness from the acquired light fringes using a self-written MATLAB code, while repeating each measurement at least three times to assess variability, which was found to be small owing to the well-defined conditions of the experiments. In particular, the variability of the steady film thickness under the same excitation level
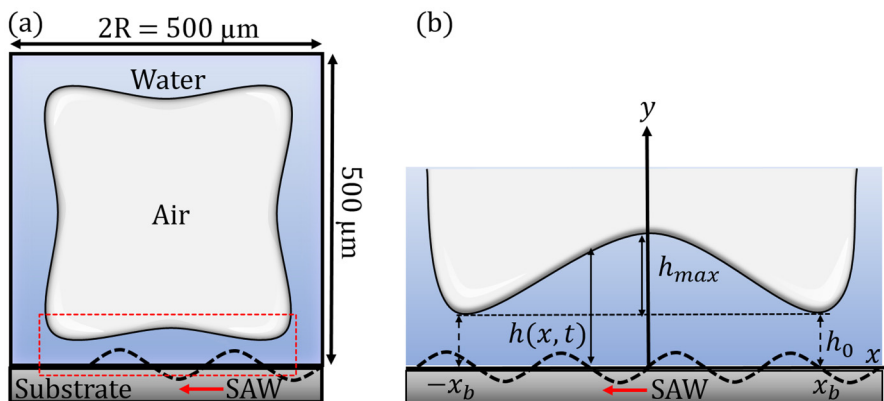
FIG. 2. (a) A cross-section sketch of the experimental system whose area of interest, where we examine the contribution of SAWs to the stability of the liquid film between a bubble and a channel wall, is given in a red dashed square and is magnified in (b). We define the difference between the maximum and minimum ($h_0$) film thicknesses to be $h_{\max}$. The two initial minima of the film are symmetric with respect to its maximum so that we define their positions as $\pm x_b$ with respect to the position of the film maximum along the substrate.

is within the limits of the measurement error of 110 nm. Further details about the reconstruction code are given elsewhere [20].

## III. RESULTS AND DISCUSSION

In the absence of SAWs, capillary forces which support an excess Laplace pressure in the bubble, encourage the drainage of a water intervening film between the bubble and the microchannel walls. Contrary to the case of 100-$\mu$m-thick channels, where we observe the fast dewetting of the channel walls in a matter of seconds (not shown here), in the case of 500-$\mu$m-thick channels we do not observe dewetting at the time of the experiment. Instead, we observe the continuous thinning of the intervening film between the bubble and the microchannel walls, which is shown in Fig. 3. The same channels are used to explore the SAW contribution to the dynamics of the liquid film.
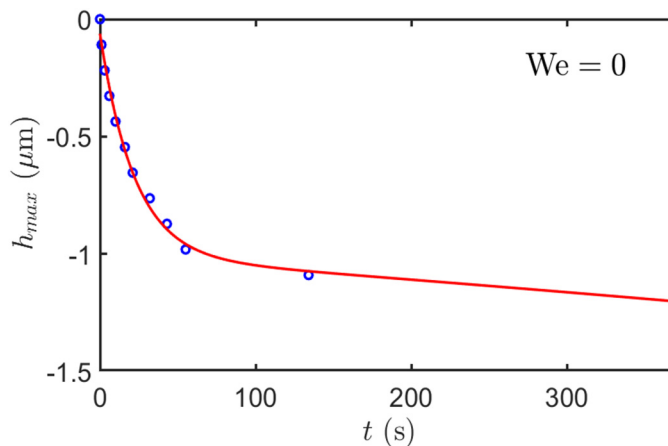


FIG. 3. Temporal evolution of the maximal film thickness, $h_{\max}$, with respect to its initial value, obtained in experiment in the absence of SAW excitation, where the blue circles are measurements and the red solid line is a guide to the eye.

Exciting SAWs in the bottom substrate of the 500-$\mu$m-thick channels, we observed that the film thickness may thin or thicken, until it reaches a steady geometry. To quantify the contribution of the acoustic power to the evolution of the intervening film we employ the acoustic Weber number [17],

$$\mathrm{We_s} \equiv \chi \rho U^2 \delta /(\gamma \epsilon^3) = \chi \rho U^2 R/(\gamma \epsilon), \tag{1}$$

which reflects the ratio between the acoustic stress, $\chi \rho U^2$, and the capillary stress, $\gamma/R$, in the liquid film. The term *acoustic stress* is associated with the stress which is generated in the liquid due to the presence of the acoustic wave in the neighboring solid. The term *capillary stress* is associated with the stress in the liquid which results from the surface tension and the curvature of the liquid-air interface. Further, $\epsilon \equiv \sqrt{\delta/R} \ll 1$ is a lubrication parameter which quantifies the ratio between the viscous penetration length of the SAW into water, $\delta \equiv \sqrt{2\mu/\rho\omega} \approx 130$ nm, and the radius of curvature of the menisci at the corners of the channel, which is proportional to the Laplace pressure in the bubble. We approximate the radius of curvature as half the channel thickness ($R \approx 250$ $\mu$m). Moreover, the parametric values that we employ are $\chi \approx 1.3$, $\rho \approx 1000$ kg/m$^3$, $\gamma \approx 70$ mN/m, $\mu \approx 1$ mPa s, and $\omega \approx 2\pi \times 20$ MHz, which denote the factor by which the SAW longitudinal particle-velocity amplitude at the solid surface is smaller than its transverse counterpart for a Rayleigh SAW [34], the density of water, the surface tension at the air/water interface, the viscosity of water, and the angular frequency of the SAW, respectively.

The absolute film thickness, $h$, cannot be measured quantitatively by means of light microscopy. Our results give the spatial thickness of the film, $\tilde{h} \equiv h - h_0$, relative to a minimum film thickness $h_0$. The upper limit for the magnitude of $h_0$ at long times and in the absence of SAWs, e.g., Fig. 3, is the error of measurement of the draining film thickness, which is given by $\lambda/4 \approx 110$ nm, where $\lambda$ is the wavelength of the monochromatic light. Drainage measurements in the absence of SAWs further indicate that the initial maximum film thickness in the different experiments is approximately $\tilde{h} \approx 1$–1.5 $\mu$m, when considering the decay in the rate of the film thinning at long times. A similar conclusion is obtained from the spatial variation in film thickness at short times, e.g., Fig. 4, where we present the evolution of the film thickness, $\tilde{h}$, for different levels of acoustic excitation.

We show in Fig. 4(a) that at $\mathrm{We_s} = 0.6$, the intervening film thins as liquid drains out of the film, where the uppermost curve corresponds to the moment at which the acoustic power was commenced. In Fig. 4(b), we show the evolution of the film thickness at $\mathrm{We_s} = 1.7$, which results in an increase in the film thickness, where the lowermost curve corresponds to the moment at which the acoustic power was commenced. The films in both cases appear to attain a steady thickness. These results indicate the stabilizing action of the SAW on the film thickness when compared to the thinning of the film in the absence of SAW in Fig. 3, where we observe the continuous thinning of the film by more than 1 $\mu$m over several minutes.

In Fig. 5 we show the temporal evolution of the maximum film thickness for various values of $\mathrm{We_s}$. The excitation of a propagating SAW commences at $t = 0$. Before this time the liquid in the film undergoes spontaneous drainage and the film thins under the action of the Laplace pressure in the bubble. Under the different levels of SAW excitation in our measurements, the films appear to attain a stable thickness after approximately 20 s from the time we commenced the application of the SAW. The same observation is true even when the acoustic Weber number is below its theoretical threshold value for film stability, $\mathrm{We_s} < 1.49$. At $\mathrm{We_s} \geqslant 1.33$, the films in our experiments appear to thicken toward a steady thickness level. At $\mathrm{We_s} \leqslant 0.85$ the films thin toward a steady thickness level. In both cases the films avoid the fast film destabilization observed previously in the corresponding case of silicon oil for $\mathrm{We_s} < 1.49$ or the continuous thinning observed for water films in the absence of SAW excitation (shown in Fig. 3).

Our results do not conform to the findings of the theory for the acoustic Landau-Levich coating film. According with the theory, the film should become unstable when $\mathrm{We_s} < 1.49$, which was observed in the case of silicon oil [20]. In our current water experiments, the films appear to approach stable thicknesses both above and below the film stability threshold value of $\mathrm{We_s}$ (in the presence of acoustic power). In particular, when decreasing the magnitude of $\mathrm{We_s}$, the dynamics of the water films approach the limit of a continuous film drainage in the absence of SAW excitation,
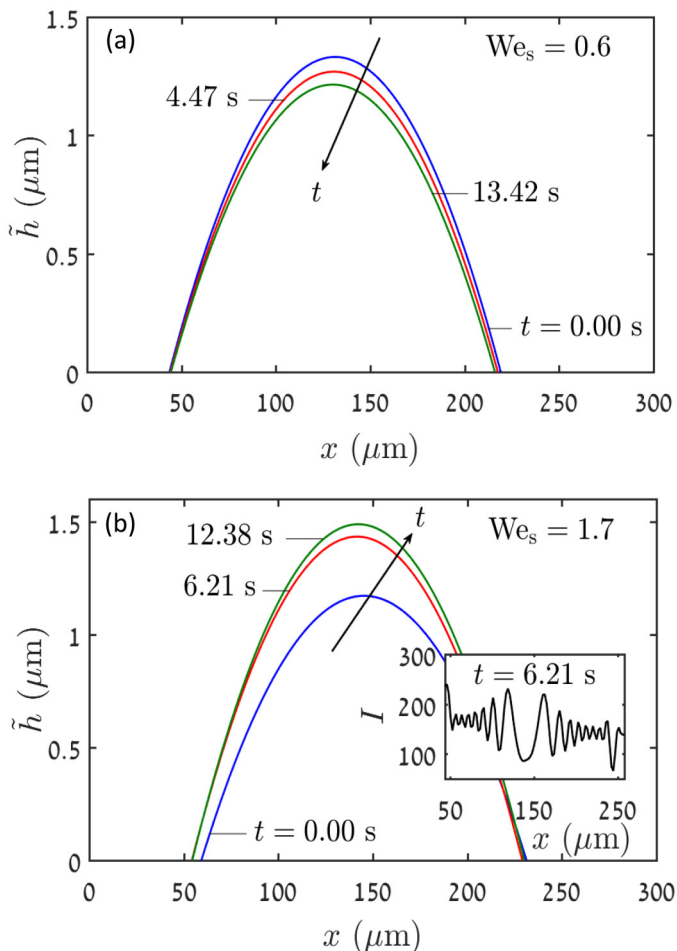
FIG. 4. Thickness ($\tilde{h} \equiv h - h_0$) evolution of an intervening film in a cross-section view at different times for the cases of low and high acoustic power, where $t = 0$ corresponds to the time of commencement of acoustic power, when the minima of the films correspond initially to the positions $\pm x_b$ in Fig. 2 and the error of measurement in film thickness is approximately a quarter of the light wavelength, that is, approximately 110 nm. In the inset we show a pixel intensity profile, which was extracted from an experimental image, such as the one in Fig. 1(b) at the dashed white line, and according to which we reconstructed the film thickness.

e.g., Fig. 3. We do not observe the fast collapse of water films, which was previously monitored in the case of silicon oil in the unstable regime of the theory for the acoustic Landau-Levich coating film.

The different hydrodynamic parameters and surface tension levels in the current experiments with water and in the previous experiments with silicon oil are accounted for in the parameter $\mathrm{We_s}$. Hence, our findings may point to the presence of an additional fundamental difference between the response of thin films of oil and water to SAWs.

A recent theoretical study [21] may suggest a solution to the controversy observed between the response of thin films of water and silicon oil to the SAW excitation in our analysis. The theory finds that the presence of an excess pressure in the liquid film due to long range surface forces, which traverse the film thickness at least where the film becomes thin (the precursor film in the case of a Landau-Levich coating film), will alter film dynamics. The presence of the surface forces is
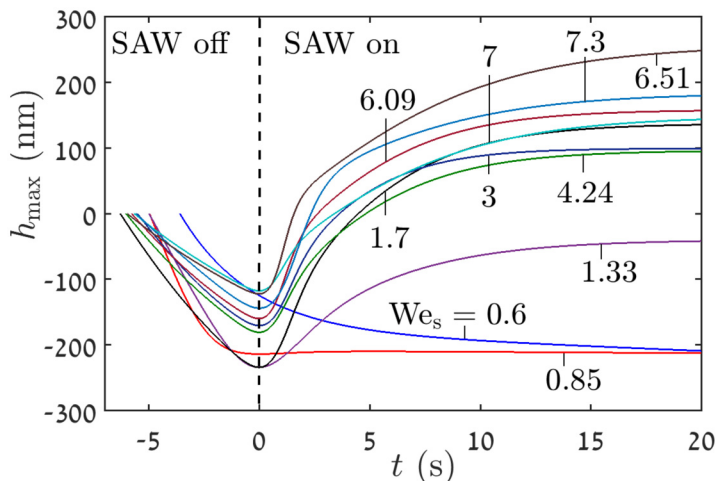
FIG. 5. Temporal evolution of the maximal film thickness, $h_{max}$, with respect to the initial value obtained in experiment for various values of $We_s$, where $t = 0$ corresponds to the commencement of acoustic power and the error of measurement in film thickness is a quarter of the monochromatic light wavelength of approximately 110 nm. The different films approach a finite steady thickness approximately 20 s from the time of commencement of acoustic power.

anticipated to stabilize the SAW excited coating film regardless of the level of acoustic excitation and avoid the fast collapse of the film at small levels of acoustic power, which was observed in the case of oil films. Moreover, a fundamental difference between oil and water films is the presence of electrical double layers (EDLs) of ions near the surfaces of the film, which naturally become charged in water. The collision of EDLs of ions when the film is thin, i.e., when the upper and lower surfaces of the film are close, generates an excess electrical and osmotic pressure in the film.

Both the air/water interface and the oxide surface of lithium niobate are negatively charged at the experimental conditions. The former interface mentioned obtains $\zeta$ potential levels in the range of $-30$ to $-50$ mV at the experimental conditions [35,36], and the latter interface was measured to obtain a $\zeta$ potential of $-98$ mV in the absence of SAWs [37]. Hence, the collision of the opposing EDLs of ions generates a positive excess pressure in the film. Moreover, in the absence of added electrolyte in our experiments, the deionized water shows a pH level of 5.66, which is compatible with the dissolution of carbon dioxide, $CO_2$, at atmospheric pressure and its transformation to carbonic acid [38]. The dissolution of carbon dioxide in water increases the acidity of the water solution according to the chemical formula $CO_2 + H_2O \rightleftarrows H_2CO_2 \rightleftarrows HCO_3^- + H^+ \rightleftarrows CO_3^{2-} + 2H^+$, where the majority of ions in the solution are associated with the species $HCO_3^-$ and $H^+$. The corresponding Debye length, which characterizes the exponential decay length of the EDL is given to leading order by [39] $\kappa^{-1} \approx 0.3\,(nm\sqrt{M})/\sqrt{I\,(M)} \approx 203$ nm (units in the previous formula are given in brackets), where $I \approx 10^{-5.66}M$ is the ionic strength in water at the given pH level, and "$M$" is the concentration unit of "molar" or "gram mole/liter." Hence, the submicron components of the water films in our experiments experience a weak excess EDL pressure. The low level of ionic strength renders the EDL pressure in the film small and unlikely to overcome the Laplace pressure in the bubble by itself. However, alongside SAW actuation, it may be sufficient to alter the dynamics of the liquid film. Further dedicated theory and experiment are required to scrutinize this assertion.

## IV. CONCLUSIONS

In this study we examine the contribution of megahertz-frequency SAWs in a solid substrate to the stability of a water film above. We employ the micron- and submicron-thick films that appear

between long bubbles and the wall of a microfluidic channel whose substrate is comprised from a piezoelectric acoustic actuator (a SAW device). Previous theoretical work on the stability of the acoustic Landau-Levich coating problem predicts that a film thickness should be stabilized and destabilized by the SAW when the ratio between acoustic and capillary stresses, which is quantified by an acoustic Weber number, is above and below a threshold value of approximately $We_s \approx 1.49$, respectively. In a previous study, the theory was found to compare quantitatively to experiment in the case where the SAW actively destabilizes silicon oil films.

Here we show that the SAW stabilizes water films at sufficiently large acoustic power levels, which are commensurate with the stable regime of the acoustic Landau-Levich coating problem. However, we observe that the water films further appear stabilized by the SAW in the unstable regime of the acoustic Landau-Levich coating problem. In the latter case, the water films appear to avoid the fast collapse, which was observed previously in the case of silicon films under the unstable regime, and the continuous thinning, which was observed in the case of water films in the absence of SAW excitation. Our observations indicate a fundamental difference between the response of thin films of oil and water to SAW excitation. In particular, the hydrodynamic and surface tension properties of both liquids are taken into account in the only dimensionless parameter in the theory for the acoustic Landau-Levich coating problem, $We_s$ [17].

A different theoretical study [21] suggests a solution to the controversy observed in our experiment. It appears that the presence of an excess pressure in the liquid film due to long range surface forces will stabilize the SAW excited Landau-Levich coating film in the case where $We_s < 1.49$. Hence, the modified theory highlights the absence of the SAW-induced fast collapse regime of the film, i.e., the absence of the unstable regime in the acoustic Landau-Levich problem, in the presence of long range repulsive surface forces in the film.

Unlike oil films, water films support EDLs of ions near the solid/water and air/water interfaces. The thickness of the film at which the excess EDL pressure becomes appreciable is the Debye length of the EDL, which is given approximately by $\kappa^{-1} \approx 203$ nm in our experiments. It is of a similar order of magnitude to the submicron thickness levels of the measured water films. Hence, both the presence of the long range EDL excess pressure in water films and the absence of the SAW-induced fast collapse (unstable regime) in our experiments appear to be consistent with the assumptions and results of the modified theory. It is left for future studies to elucidate and quantify the mutual contributions of the EDLs and SAWs to film dynamics.

[1] R. F. Tabor, R. Manica, D. Y. C. Chan, F. Grieser, and R. R. Dagastine, Repulsive van der Waals Forces in Soft Matter: Why Bubbles Do Not Stick to Walls, Phys. Rev. Lett. **106**, 064501 (2011).

[2] R. R. Dagastine, R. Manica, S. L. Carnie, D. Y. C. Chan, G. W. Stevens, and F. Grieser, Dynamic forces between two deformable oil droplets in water, Science **313**, 210 (2006).

[3] R. R. Dagastine and L. R. White, Forces between a rigid probe particle and a liquid interface: II. The general case, J. Colloids Interface Sci. **247**, 310 (2002).

[4] J. Kohnle, G. Waibel, R. Cernosa, M. Storz, H. Ernst, H. Sandmaier, T. Strobelt, and R. Zengerle, A unique solution for preventing clogging of flow channels by gas bubbles, in *Fifteenth Conference on Micro Electro Mechanical Systems* (IEEE, New York, 2002), pp. 77–80.

[5] O. Manor, I. Vakarelski, X. Tang, S. O'shea, G. Stevens, F. Grieser, R. Dagastine, and D. Y. C. Chan, Hydrodynamic Boundary Conditions and Dynamic Forces between Bubbles and Surfaces, Phys. Rev. Lett. **101**, 024501 (2008).

[6] O. Manor, I. U. Vakarelski, G. W. Stevens, F. Grieser, R. R. Dagastine, and D. Y. C. Chan, Dynamic forces between bubbles and surfaces and hydrodynamic boundary conditions, Langmuir **24**, 11533 (2008).

[7] C.-Y. Lin and J. C. Slattery, Thinning of a liquid film as a small drop or bubble approaches a solid plane, AIChE J. **28**, 147 (1982).

[8] C. Litterst, T. Metz, R. Zengerle, and P. Koltay, Static and dynamic behaviour of gas bubbles in T-shaped non-clogging micro-channels, Microfluid. Nanofluid. **5**, 775 (2008).

[9] A. Hibara, S. Iwayama, S. Matsuoka, M. Ueno, Y. Kikutani, M. Tokeshi, and T. Kitamori, Surface modification method of microchannels for gas-liquid two-phase flow in microchips, Anal. Chem. **77**, 943 (2005).

[10] J. Xu, R. Vaillant, and D. Attinger, Use of a porous membrane for gas bubble removal in microfluidic channels: Physical mechanisms and design criteria, Microfluid. Nanofluid. **9**, 765 (2010).

[11] H. G. Derami, R. Vundavilli, and J. Darabi, Experimental and computational study of gas bubble removal in a microfluidic system using nanofibrous membranes, Microsyst. Technol. **23**, 2685 (2017).

[12] W. Zheng, Z. Wang, W. Zhang, and X. Jiang, A simple PDMS-based microfluidic channel design that removes bubbles for long-term on-chip culture of mammalian cells, Lab Chip **10**, 2906 (2010).

[13] C. Lochovsky, S. Yasotharan, and A. Günther, Bubbles no more: In-plane trapping and removal of bubbles in microfluidic devices, Lab Chip **12**, 595 (2012).

[14] D. L. Chen, L. Li, S. Reyes, D. N. Adamson, and R. F. Ismagilov, Using three-phase flow of immiscible liquids to prevent coalescence of droplets in microfluidic channels: Criteria to identify the third liquid and validation with protein crystallization, Langmuir **23**, 2255 (2007).

[15] S. H. Tan, N. T. Nguyen, Y. C. Chua, and T. G. Kang, Oxygen plasma treatment for reducing hydrophobicity of a sealed polydimethylsiloxane microchannel, Biomicrofluidics **4**, 32204 (2010).

[16] K. Ohtani, M. Tsuchiya, H. Sugiyama, T. Katakura, M. Hayakawa, and T. Kanai, Surface treatment of flow channels in microfluidic devices fabricated by stereolithography, J. Oleo Sci. **63**, 93 (2014).

[17] M. Morozov and O. Manor, An extended Landau-Levich model for the dragging of a thin liquid film with a propagating surface acoustic wave, J. Fluid Mech. **810**, 307 (2017).

[18] G. Altshuler and O. Manor, Spreading dynamics of a partially wetting water film atop a MHz substrate vibration, Phys. Fluids **27**, 102103 (2015).

[19] G. Altshuler and O. Manor, Free films of a partially wetting liquid under the influence of a propagating MHz surface acoustic wave, Phys. Fluids **28**, 072102 (2016).

[20] A. Horesh, M. Morozov, and O. Manor, Enhanced drainage and thinning of liquid films between bubbles and solids that support surface waves, Phys. Rev. E **95**, 052803 (2017).

[21] K. D. J. Mitas, O. Manor, and U. Thiele, Bifurcation study for a surface-acoustic-wave driven meniscus, arXiv:2006.12113.

[22] M. K. Tan, J. R. Friend, and L. Y. Yeo, Microparticle collection and concentration via a miniature surface acoustic wave device, Lab Chip **7**, 618 (2007).

[23] P. Garstecki, M. J. Fuerstman, H. A. Stone, and G. M. Whitesides, Formation of droplets and bubbles in a microfluidic T-junction—scaling and mechanism of break-up, Lab Chip **6**, 437 (2006).

[24] FEMTOPCCE, Diener Electronic.

[25] Rohde & Schuarz, SMB-300.

[26] Tabor Electronics Ltd., A10150.

[27] Polytec Inc., MSA-500.

[28] J. Friend and L. Y. Yeo, Microscale acoustofluidics: Microfluidics driven via acoustics and ultrasonics, Rev. Mod. Phys. **83**, 647 (2011).

[29] New Era Pump System Inc., NE-100, and Chemyx Inc., Model Fusion 740, respectively.

[30] Nikon Eclipse Ti-S.

[31] Nikon Plan Fluor.

[32] Nikon DS-Qi2.

[33] H. Wong, C. J. Radke, and S. Morris, The motion of long bubbles in polygonal capillaries. Part 1. Thin films, J. Fluid Mech. **292**, 71 (1995).

[34] D. Royer and E. Dieulesaint, *Elastic Waves in Solids I* (Springer-Verlag, Berlin, 1996).

[35] M. Manciu and E. Ruckenstein, Ions near the air/water interface: I. Compatibility of zeta potential and surface tension experiments, Colloids Surf. A **400**, 27 (2012).

[36] M. Flury and S. Aramrak, Role of air-water interfaces in colloid transport in porous media: A review, Water Resour. Res. **53**, 5247 (2017).

[37] Using a SurPASS electrokinetic analyzer for solid surfaces, Anton Paar GmbH.

[38] H. T. Byck, Effect of dissolved $CO_2$ on the pH of water, Science **75**, 224 (1938).

[39] J. N. Israelachvili, *Intermolecular and Surface Forces* (Academic Press, New York, 2015).